Observation of topological transitions in interacting quantum circuits

P. Roushan[1],* C. Neill[1],* Yu Chen[1],* M. Kolodrubetz[2], C. Quintana[1], N. Leung[1], M. Fang[1], R. Barends[1], B. Campbell[1], Z. Chen[1], B. Chiaro[1], A. Dunsworth[1], E. Jeffrey[1], J. Kelly[1], A. Megrant[1], J. Mutus[1], P. O'Malley[1], D. Sank[1], A. Vainsencher[1], J. Wenner[1], T. White[1], A. Polkovnikov[2], A. N. Cleland[1], and J. M. Martinis[1†]
[1]*Department of Physics, University of California, Santa Barbara, CA 93106-9530, USA and*
[2]*Department of Physics, Boston University, Boston, MA 02215, USA*

The discovery of topological phases in condensed matter systems has changed the modern conception of phases of matter [1, 2]. The global nature of topological ordering makes these phases robust and hence promising for applications [3]. However, the non-locality of this ordering makes direct experimental studies an outstanding challenge, even in the simplest model topological systems, and interactions among the constituent particles adds to this challenge. Here we demonstrate a novel dynamical method [4] to explore topological phases in both interacting and non-interacting systems, by employing the exquisite control afforded by state-of-the-art superconducting quantum circuits. We utilize this method to experimentally explore the well-known Haldane model of topological phase transitions [5] by directly measuring the topological invariants of the system. We construct the topological phase diagram of this model and visualize the microscopic evolution of states across the phase transition, tasks whose experimental realizations have remained elusive [6, 7]. Furthermore, we developed a new qubit architecture [8, 9] that allows simultaneous control over every term in a two-qubit Hamiltonian, with which we extend our studies to an interacting Hamiltonian and discover the emergence of an interaction-induced topological phase. Our implementation, involving the measurement of both global and local textures of quantum systems, is close to the original idea of quantum simulation as envisioned by R. Feynman [10], where a controllable quantum system is used to investigate otherwise inaccessible quantum phenomena. This approach demonstrates the potential of superconducting qubits for quantum simulation [11, 12] and establishes a powerful platform for the study of topological phases in quantum systems.

Since the first observations of topological ordering in quantum Hall systems in the 1980s [1, 2], experimental studies of topological phases have been primarily limited to indirect measurements. The non-local nature of topological ordering renders local probes ineffective, and when global probes, such as transport, are used, interpretations [13] are required to infer topological properties from the measurements. Topological phases are characterized by topological invariants, such as the first Chern number $\mathcal{C}\hbar$, whose discrete jumps indicate transitions between different topologically ordered phases [14, 15]. For a quantum system, $\mathcal{C}\hbar$ is defined as the integral over a closed manifold $\mathcal{S}$ in the parameter space of the Hamiltonian as

$$\mathcal{C}\hbar \equiv \frac{1}{2\pi}\oint_{\mathcal{S}} \mathbf{B}\cdot d\mathcal{S}, \tag{1}$$

where $\mathbf{B}$ is the Berry curvature [16–18]. As illustrated in Fig. 1 and discussed in the supplement, $\mathbf{B}$ can be viewed as an effective magnetic field with points of ground state degeneracy acting as its sources, i.e. magnetic monopoles [17, 19]. Using Gauss's law for the Berry curvature (magnetic field), $\mathcal{C}\hbar$ simply counts the number of degenerate energy eigenvalues (magnetic monopoles) enclosed by the parameter manifold $\mathcal{S}$. $\mathcal{C}\hbar$, which is invariant under perturbations to the shape of $\mathcal{S}$, is a topological number that reflects a property of the manifold of states as a whole and not a local property of parameter space.

In previous works, topological properties of highly symmetric quantum systems have been measured [20–22]. However, since these earlier studies relied on interference to evaluate the accumulated phase, these methods are not readily generalizable. To circumvent this, Gritsev et

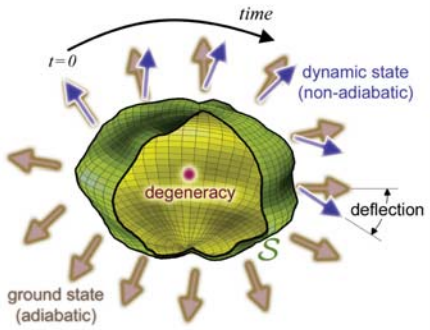

Figure 1. **Dynamical measurement of Berry curvature and $\mathcal{C}\hbar$.** In this schematic drawing, brown arrows represent the ground states (adiabatic limit) for given points on a closed manifold $\mathcal{S}$ (green enclosure) in the parameter space, and the blue arrows are the measured states during a non-adiabatic passage. According to (2), the Berry curvature $\mathbf{B}$ can be calculated from the deviation from adiabaticity. Integrating $\mathbf{B}$ over $\mathcal{S}$ gives the Chern number $\mathcal{C}\hbar$, which corresponds to the total number of degeneracies enclosed.

al. [4] proposed a general method to directly measure the local Berry curvature. The underlying physics of their idea is that motion in a curved space will be deflected from a straight trajectory; in other words, curvature reveals itself as an effective force. For example, a charged particle moving in a magnetic field experiences the well-known Lorentz force. Similarly, Gritsev et al. showed that in a region of the parameter space with Berry curvature $\mathbf{B}$, if we "move" a quantum system by changing a parameter of its Hamiltonian with rate v, then the state of the system feels a force $\mathbf{F}$ given by

$$\mathbf{F} \propto v \times \mathbf{B} + O(v^2). \tag{2}$$

This force leads to deviations of the trajectory from the adiabatic path which can be detected through measurements of the observables in the quantum system (see Fig. 1 and [17]). Therefore, as long as the ramping of parameters is done slowly, but not necessarily adiabatically, the deviation is directly proportional to $\mathbf{B}$. As the adiabatic limit is generally hard to achieve, this relation has the important advantage of needing only a moderately slow change of state and only requires that the linear term in (2) dominates the dynamics.

This dynamical method suggests a way to directly measure $\mathbf{B}$, from which $\mathcal{C}\hbar$ can be calculated using (1). This provides an alternative means to study topological phases, significantly different from conventional approaches. Admittedly, implementing this procedure requires the ability to continually change the system Hamiltonian, which is difficult to do in most experimental situations. However, in a fully controllable quantum system, this provides a powerful means to probe the topological properties of the ground state manifold through dynamical measurements. Here we demonstrate an implementation of this type of measurement using a quantum circuit based on superconducting qubits [11, 12, 23].

We first demonstrate a basic implementation of the dynamical method. The quantum state of a single superconducting qubit [17, 24] is equivalent to a spin-1/2 particle in a magnetic field. Its Hamiltonian can be written as

$$\mathcal{H}_S = -\frac{\hbar}{2}\mathbf{H}\cdot\boldsymbol{\sigma}, \tag{3}$$

where $\boldsymbol{\sigma} = (\sigma^x, \sigma^y, \sigma^z)$ are the Pauli matrices, and $\mathbf{H} = (H_X, H_Y, H_Z)$ is analogous to a control magnetic field. Full control over the parameters of this Hamiltonian is achieved by microwave pulses that control H_X and H_Y, and an applied flux through the qubit's SQUID loop which controls H_Z. To illustrate the dynamical method, we measure $\mathcal{C}\hbar$ for a spherical ground state manifold in $\mathbf{H}$-parameter space (Fig. 2). We use θ and ϕ as spherical coordinates and consider the parameter trajectory starting at the north pole at $t = 0$ and ramps along the $\phi = 0$ meridian ($H_Y = 0$) with constant velocity $v_\theta = d\theta/dt$ until it reaches the south pole at $t = T_f$. To realize

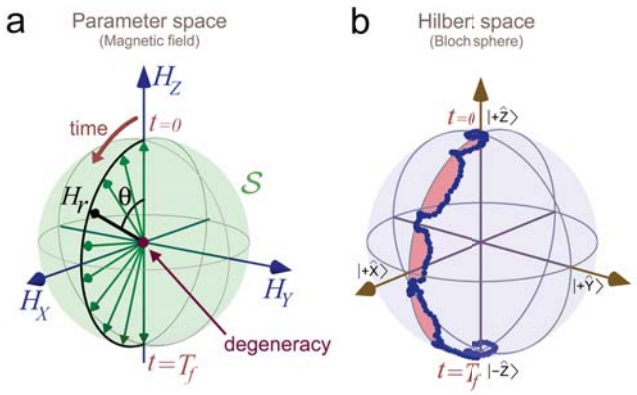

Figure 2. **Dynamical measurement of $\mathcal{C}\hbar$. a.** A simultaneous microwave pulse $H_X(t) = H_r \sin(\pi t/T_f)$ and detuning pulse $H_Z(t) = H_r \cos(\pi t/T_f)$ are applied to construct a parameter space trajectory. The pulse sequence results in a parameter space motion along the $\phi = 0$ meridian ($H_Y = 0$ plane) on $\mathcal{S}$. **b.** The state of the qubit during this ramp ($H_r/2\pi = 10$ MHz and $T_f = 600$ ns) is determined using tomography [17], and shown (blue dots) on the surface of the Bloch sphere.

motion on a spherical manifold, the control sequences of H_Z and H_X are chosen such that the control magnitude $|\mathbf{H}| = H_r$ is constant [17]. In the adiabatic limit, the wavefunction would remain in the instantaneous ground state of $\mathcal{H}_S$, with the Bloch vector parallel to the direction of the control field, following the meridian. Instead, for non-adiabatic ramps, a deviation from the meridian is observed, as shown in Fig. 2(b). Here the Bloch vector is measured at each point in time by interrupting the ramp and performing state tomography. Note that this deviation is not due to noise, but rather is the expected non-adiabatic response [17]. For this trajectory, the force $\mathbf{F}$ takes the form $f_\phi = \frac{\hbar}{2} H_r \langle\sigma^y\rangle \sin\theta$, where $\langle\sigma^y\rangle$ is the expectation value of σ^y. Integrating over the resulting deflection (shaded light red in Fig. 2(b)) gives $\mathcal{C}\hbar = 1 \pm 0.05$. Note that given the symmetry of the Hamiltonian, a line integral is sufficient for measuring the surface integral of $\mathcal{C}\hbar$ (see (1)) [17, 25]. A value of unity is expected, as the qubit ground state has a single degeneracy at $\mathbf{H} = 0$, corresponding to an effective monopole, the enclosing parameter sphere $\mathcal{S}$ should yield $\mathcal{C}\hbar = 1$. In the supplement we demonstrate the robustness of $\mathcal{C}\hbar$ by deforming the surface manifold $\mathcal{S}$ and discuss the sources of error,[26].

Using our controllable quantum circuit, we can explore what is perhaps the simplest model of topological behavior in condensed matter, the Haldane model [5, 17]. This model serves as a foundation for other topological insulator models [27–29], yet its experimental realization has remained elusive [6, 7]. To show that the quantum Hall effect could be achieved without a global magnetic field, Haldane introduced a non-interacting Hamiltonian on a

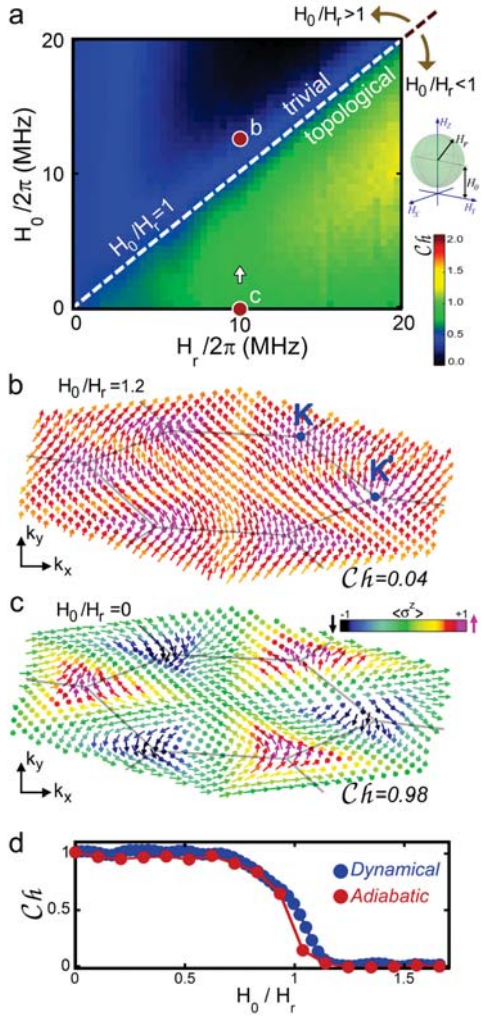

Figure 3. **Dynamic measurement of the topological phase diagram and adiabatic visualization of phases. a.** Dynamical determination of the phase diagram. first $\langle\sigma^y\rangle$ was measured during ramps similar to those in Fig 2(a), and then $\mathcal{C}\hbar$ was calculated. The dashed line is the expected phase boundary at $H_0 = H_r$. **b,c.** With adiabatic state preparation, the state of the qubit was prepared and measured over a grid on the surface of the parameter sphere and then mapped to the hexagonal momentum-space plane. The ground states are presented as Bloch vectors, whose colors indicate their $\langle\sigma^z\rangle$ values. $H_0/H_r = 1.2$ for **b** and $H_0/H_r = 0$ for **c**. The gray lines show the FBZ of the honeycomb lattice and high symmetry points **K** and **K′** are marked. **d.** The measured $\mathcal{C}\hbar$ from the adiabatic and dynamical (white arrow in **a**) methods are plotted vs. H_0/H_r.

honeycomb lattice [5] given by

$$\mathcal{H}_G(k_x, k_y) = \hbar v_F(k_x\sigma^x + k_y\sigma^y) + (m_0 - m_t)\sigma^z, \quad (4)$$

where v_F is the Fermi velocity, m_0 is the effective mass, and m_t corresponds to a second-neighbor hopping in a local magnetic field. The key prediction of the Haldane model is that if $m_0/m_t > 1$ the system is in a trivial insulating phase, and otherwise in a topological phase, where edge states and quantized conductance appear. Using a confocal mapping [17] one can recast Eq. (4) into the single-qubit Hamiltonian (3). If we consider spherical manifolds $\mathcal{S}$ of radius H_r displaced from the origin in the z direction by H_0, then H_0/H_r in the qubit system plays the same role as m_0/m_t in the Haldane model. In Fig. 3(a) we plot the results of this measurement, showing $\mathcal{C}\hbar$ as a function of H_r and H_0, which shows plateaus at values 0 and 1 separated by a phase transition boundary line at $H_r = H_0$. This transition can be easily understood: when $H_0 < H_r$ the degeneracy at $\mathbf{H} = 0$ lies within the sphere giving $\mathcal{C}\hbar = 1$, whereas for $H_0 > H_r$ it lies outside the sphere giving $\mathcal{C}\hbar = 0$.

The nature of the topological and trivial phases can be further revealed by probing their microscopic structure with a conventional adiabatic method. According to Haldane, each phase has its own signature spin texture in momentum space. We again consider spherical surfaces $\mathcal{S}$ and adiabatically ramp the control parameters to their final values on $\mathcal{S}$. The resulting Bloch vectors are then tomographically measured [17], and ideally point in the same direction as the final $\mathbf{H}$. With a confocal mapping (see [17]), $\mathcal{S}$ can be mapped to the first Brillouin zone (FBZ) of the honeycomb lattice. Therefore, the adiabatically measured ground state vectors on $\mathcal{S}$ can be depicted in the FBZ. Fig. 3(b) and (c) show the results for two manifolds with $H_0/H_r = 1.2$ and 0, corresponding to trivial and topological phases, respectively. By following the orientation of the state-vector along any path starting at $\mathbf{K}$ and moving to $\mathbf{K}'$ (corners of the FBZ) and back to $\mathbf{K}$ one can see that in the topological case the state vector makes one full rotation, while in the trivial case and only tilts away from vertical and then returns, without completing a rotation. These spin texture maps can be used to extract local Berry curvature [17]. As shown in Fig. 3(c), the resulting $\mathcal{C}\hbar$ from this adiabatic method shows good agreement with the dynamical method of measurement.

Moving beyond the realm of non-interacting systems, we now study the topological phase diagram for an interacting Hamiltonian, obtained by measuring $\mathcal{C}\hbar$ in a coupled two-qubit system. The intriguing physics of the topological properties of this kind of interacting system has to date been mostly unexplored, due to experimental challenges. One significant source of challenge is that one needs full control over the entire parameter space, including over any coupling terms in the Hamiltonian. Here we achieve this kind of full control by using a new design for our superconductong qubit, which includes the ability to continuously vary the inter-qubit coupling strength g (we term this new type of qubit the "gmon" [8, 9]).

The Hamiltonian of this system is given by

$$\mathcal{H}_{2Q} = -\frac{\hbar}{2}[H_0\sigma_1^z + \mathbf{H_1}\cdot\boldsymbol{\sigma_1} + \mathbf{H_2}\cdot\boldsymbol{\sigma_2} - g(\sigma_1^x\sigma_2^x + \sigma_1^y\sigma_2^y)], \quad (5)$$

where 1 and 2 refer to qubit 1 (Q1) and qubit 2 (Q2)

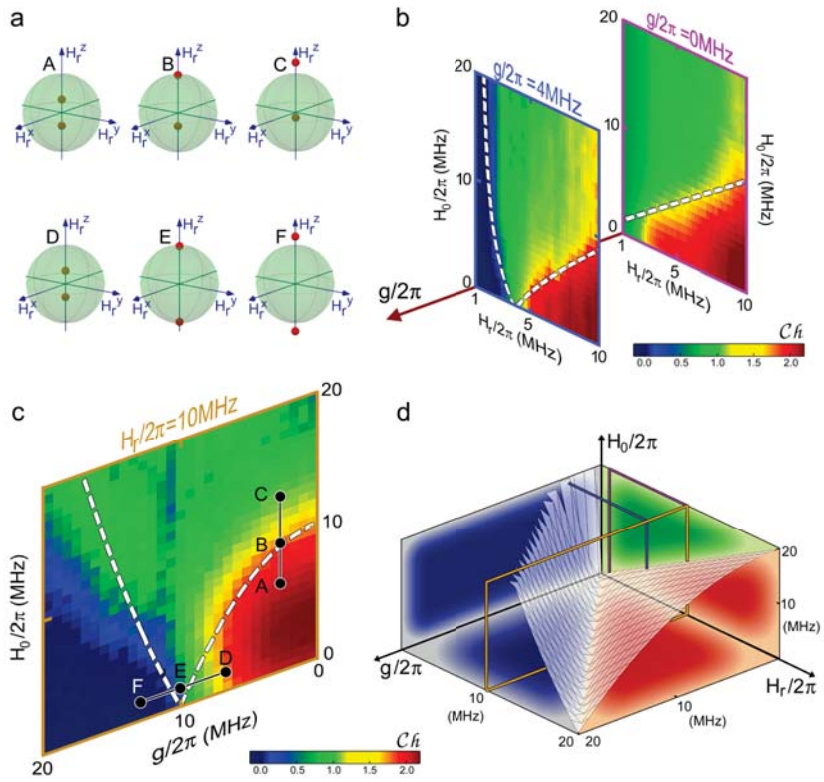

Figure 4. **Topological phase diagram of an interacting system. a.** The position of the monopoles in H-space for the points A through F shown in panel **c**, with a spherical manifold of radius $H_r/2\pi = 10$ MHz. **b,c.** The topological phase diagram of Eq. (5). In panel **b**, $\mathcal{C}\hbar$ was measured for two fixed $g/2\pi$ values of 0 and 4 MHz. In panel **c**, $\mathcal{C}\hbar$ was measured for fixed $H_r/2\pi$ =10 MHz. Dashed lines are topological transitions calculated analytically. **d.** The analytically calculated phase diagram showing three distinct $\mathcal{C}\hbar$ volumes and the separatrix plane. The phase diagram cuts in **b, c** are indicated by colored slices.

respectively, and the biasing field H_0 is now only applied to Q1.There are equivalent condensed matter systems to which this system can be mapped, as with the Haldane model, as discussed in [17].However, in the absence of any experimental realization of these models, our experiment is perhaps closer to Feynman's original idea of quantum simulation [10], where a controllable quantum system is used to investigate otherwise inaccessible quantum phenomena.

Using the tunable inter-qubit coupling, we can access all regions of the 7-dimensional parameter space of our Hamiltonian. Here we explore spherical manifolds with fixed $(H_0, |\mathbf{H_1}|, |\mathbf{H_2}|, g)$, analogous to the single qubit experiment.We perform experiments where both $\mathbf{H_1} = \mathbf{H_2} = \mathbf{H_r}$ are ramped simultaneously with magnitude $|\mathbf{H_r}| = H_r$, while H_0 and g are zero except during the time $t = 0$ to T_f, as illustrated in the supplement [17]. The measured $\mathcal{C}\hbar$ is shown in Fig. 4(b) and (c) for three distinct cuts though this parameter space, as shown by colored rectangles in Fig. 4(d). For $g = 0$ [panel (b)], the two qubits behave independently and the physics is the same as for the single qubit case. Since only Q1 is subject to H_0, $\mathcal{C}\hbar$ changes by 1 through the transition $H_0 = H_r$.

A new phase with $\mathcal{C}\hbar = 0$ emerges when the coupling g is large. In Fig. 4(b) for $g/2\pi = 4$ MHz, the $\mathcal{C}\hbar = 0$ phase (blue) is seen at small H_r when $H_r \lesssim g$. In Fig. 4(c) this phase also appears when $g \gtrsim H_r$, showing that the transition is interaction-driven and appears when the coupling g becomes dominant. Because (5) is not SU(2) symmetric, the results do not simply reflect the total spin of the system. However, an intuitive understanding of these phases and transitions can be attained in certain limits: at large H_r, the spins align paramagnetically with the field and add up to give $\mathcal{C}\hbar = 2$. At large g, the spins form an entangled singlet which does not respond to the applied field, giving $\mathcal{C}\hbar = 0$. Away from these limiting cases, these simple arguments are not applicable, but $\mathcal{C}\hbar$ remains quantized.

Analytic solutions predicting the phase diagram can be obtained by calculating when points with degenerate ground states cross the spherical manifold [17]. These phase boundaries are depicted in Fig. 4(d) and show three distinct regions. As discussed above, the region where g dominates (blue) has $\mathcal{C}\hbar = 0$, while where H_r dominates (red) $\mathcal{C}\hbar = 2$. There is a direct 0 to 2 transition when $H_0 = 0$, but at finite values the system first goes

through the green $\mathcal{C}\hbar = 1$ region. This latter behavior is seen in Fig. 4(c). The dashed lines in panels (b) and (c) are from this analytic solution, which uses no free parameters, and are in good agreement with the measurements. The deviations are mainly systematic errors, due to crosstalk between simultaneous control pulses. As shown in Fig. 4(a), the points of ground state degeneracy are located on the z-axis of the $\mathbf{H_r}$-space [17]. Sub-figures A, B and C correspond to the dots on Fig. 4(c), where g is small. In this limit, H_0 affects the energy of only one qubit, and increasing it moves only one monopole past the surface (C). For D, E, and F where instead H_0 is small, increasing g furthers the monopole separation, eventually moving both monopoles outside the surface (F).

An important benefit of working with a fully controllable Hamiltonian, as here, is that a number of different condensed matter systems can be mapped onto this model system. For our 2-qubit system, we show [17] that the system can be mapped to either an interacting model, or alternatively a 4-band non-interacting electron model that is a non-trivial extension of the two-band Haldane model. In general, with n qubits one can study topological phases in non-interacting 2^n-band models, an otherwise daunting experimental task. Perhaps more interesting will be to use qubit systems to study the topological phases of interacting spin-1/2 systems, where tantalizing evidence for fractionalization has been found [30].

Acknowledgments: We acknowledge fruitful discussions with R. Lutchyn, J. Moore, C. Nayak, M. Niu, A. Rahmani, T. Souza, M. Vavilov, D. Weld, and A. Yazdani. This work was supported by the NSF under grants DMR-0907039 and DMR-1029764, the AFOSR under FA9550-10-1- 0110, and the ODNI, IARPA, through ARO grant W911NF-10-1-0334. Devices were made at the UCSB Nanofab Facility, part of the NSF-funded NNIN, and the NanoStructures Cleanroom Facility.

* These authors contributed equally to this work.
† martinis@physics.ucsb.edu

[1] K. v. Klitzing, G. Dorda, and M. Pepper, "New method for high-accuracy determination of the fine-structure constant based on quantized hall resistance," Phys. Rev. Lett. **45**, 494–497 (1980).
[2] D. C. Tsui, H. L. Stormer, and A. C. Gossard, "Two-dimensional magnetotransport in the extreme quantum limit," Phys. Rev. Lett. **48**, 1559–1562 (1982).
[3] S. Das Sarma, M. Freedman, and C. Nayak, "Topological quantum computing," Physics Today **xx**, 32–38 (2006).
[4] V. Gritsev and A. Polkovnikov, "Dynamical quantum hall effect in the parameter space," PNAS **109**, 6457–6462 (2012).
[5] F. D. M. Haldane, "Model for a quantum hall effect without landau levels: Condensed-matter realization of the "parity anomaly"," Phys. Rev. Lett. **61**, 2015–2018 (1988).
[6] E. Alba, X. Fernandez-Gonzalvo, J. Mur-Petit, J. K. Pachos, and J. J. Garcia-Ripoll, "Seeing topological order in time-of-flight measurements," Phys. Rev. Lett. **107**, 235301 (2011).
[7] N. Goldman, J. Dalibard, A. Dauphin, F. Gerbier, M. Lewenstein, P. Zoller, and I. B. Spielman, "Direct imaging of topological edge states in cold-atom systems," PNAS **110**, 6736–6741 (2013).
[8] M. Geller, E. Donate, Y. Chen, C. Neill, P. Roushan, and J. M. Martinis, "Qubit architecture with high coherence and fast tunable coupling," in preparation (2014).
[9] Y. Chen, C. Neill, P. Roushan, N. Leung, M. Fang, R. Barends, J. Kelly, B. Campbell, Z. Chen, B. Chiaro, A. Dunsworth, E. Jeffrey, A. Megrant, J. Mutus, P. O'Malley, C. Quintana, D Sank, A. Vainsencher, J. Wenner, T. White, M. Geller, A. Cleland, and J. Martinis, "Qubit architecture with high coherence and fast tunable coupling," arXiv:1402.7367 (2014).
[10] R. Feynman, "Simulating physics with computers," Int. J. of Th. Phys. **21**, 467–488 (1982).
[11] A. A. Houck, H. E. Tureci, and J. Koch, "On-chip quantum simulation with superconducting circuits," Nature Physics **8**, 292–299 (2012).
[12] I. Buluta and F. Nori, "Quantum simulators," Science **326**, 108–111 (2009).
[13] D. J. Thouless, M. Kohmoto, M. P. Nightingale, and M. den Nijs, "Quantized hall conductance in a two-dimensional periodic potential," Phys. Rev. Lett. **49**, 405–408 (1982).
[14] Xiao-Gang Wen, *Quantum Field Theory of Many-body systems* (Oxford, 2004).
[15] B. A. Bernevig and T. L. Hughes, *Topological Insulators and Topological Superconductors* (Princeton University Press, 2013).
[16] This form of the Gauss's law in which the Berry curvature is treated as a 3-vector is only valid in a three-dimensional parameter space. Generalization of this logic to higher-dimensional manifolds remains work in progress.
[17] See supplementary materials and methods.
[18] M. Berry, "Quantal phase factors accompanying adiabatic changes," Proc. R. Soc. Lond. A **392**, 45–57 (1984).
[19] F. Wilczek and A. Shapere, *Geometric Phases in Physics* (World Scientific, 1989).
[20] M. Neeley, M. Ansmann, R. C. Bialczak, M. Hofheinz, E. Lucero, A. D. O'Connell, D. Sank, H. Wang, J. Wenner, A. N. Cleland, M. R. Geller, and J. M. Martinis, "Emulation of a quantum spin with a superconducting phase qudit," Science **325**, 722–725 (2009).
[21] P. J. Leek, J.M Fink, A. Blais, R. Bianchetti, M. Göppl, J. M. Gambetta, D. I. Schuster, L. Frunzio, R. J. Schoelkopf, and A. Wallraff, "Observation of berry's phase in a solid-state qubit," Science **318**, 1889–1892 (2007).
[22] M Atala, M. Aidelsburger, J. T. Barreiro, D. Abanin, T. Kitagawa, E. Demler, and I. Bloch, "Direct measurement of the zak phase in topological bloch bands," Nature Physics **9**, 795–800 (2013).
[23] M. Mariantoni, H. Wang, T. Yamamoto, M. Neeley, R. Bialczak, Y. Chen, M. Lenander, E. Lucero, A. O'Connell, D Sank, *et al.*, "Implementing the quantum von neumann architecture with superconducting circuits," Science **334**, 61–65 (2011).
[24] R. Barends, J. Kelly, A. Megrant, D. Sank, E. Jeffrey, Y. Chen, Y. Yin, B. Chiaro, J. Mutus, C. Neill, P. O'Malley, P. Roushan, J. Wenner, T. C. White, A. N. Cleland, and John M. Martinis, "Coherent josephson qubit suitable for scalable quantum integrated circuits," Phys. Rev. Lett. **111**, 080502 (2013).
[25] M. Schroer, W. Kindel, M. Kolodrubetz, M. Sandberg, M. Vissers, M. Pappas, A. Polkovnikov, and K. Lehnert, submitted (2014).
[26] C. Xu, A. Poudel, and M. G. Vavilov, "Nonadiabatic dynamics of a slowly driven dissipative two-level system," Phys. Rev. A **89**, 052102 (2014).
[27] B.A. Bernevig, T. L. Hughes, and S.-C Zhang, "Quantum spin hall effect and topological phase transition in hgte quantum wells," Science **314**, 1757–1761 (2006).
[28] M. Z. Hasan and C. L. Kane, "Colloquium: Topological insulators," Rev. Mod. Phys. **82**, 3045–3067 (2010).
[29] J.E. Moore, "The birth of topological insulators," Nature **464**, 194–198 (2010).
[30] A. Polkovnikov, unpublished (2014).